Analytica Chimica Acta 1109 (2020) 9–18

Contents lists available at ScienceDirect

Analytica Chimica Acta

journal homepage: www.elsevier.com/locate/aca

Ferrocene-labeled and purification-free electrochemical biosensor based on ligase chain reaction for ultrasensitive single nucleotide polymorphism detection

Fang Hu [a, b, 1], Wancun Zhang [c, 1], Wei Meng [b], Yuxiang Ma [a], Xianwei Zhang [c], Ying Xu [c], Peng Wang [a, **], Yueqing Gu [a, *]

[a] State Key Laboratory of Natural Medicines, Department of Biomedical Engineering, School of Engineering, China Pharmaceutical University, Nanjing, 211198, China
[b] Key Laboratory of Biomedical Functional Materials, School of Science, China Pharmaceutical University, Nanjing, 211198, China
[c] Department of Pediatric Oncology Surgery, Henan Provincial Key Laboratory of Children's Genetics and Metabolic Diseases, Children's Hospital Affiliated of Zhengzhou University, Zhengzhou, 450018, China

HIGHLIGHTS

- An Fc-labeled electrochemical biosensor was developed for SNP detection based on LCR and hybridization.
- The MT-DNA is recycled and duplicated exponentially through LCR to achieve dramatic signal amplification.
- The biosensor offers a low limit of detection (0.75 aM) and detects the allele frequency as low as 0.01%.
- The biosensor is economical, purification-free, highly-sensitive, and selective for SNPs detection.

GRAPHICAL ABSTRACT

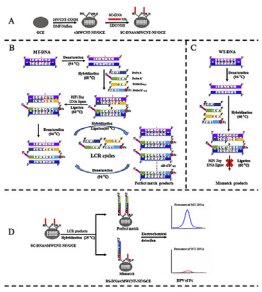

ARTICLE INFO

Article history:
Received 20 November 2019
Received in revised form
10 February 2020
Accepted 26 February 2020
Available online 27 February 2020

Keywords:
SNP
Electrochemical biosensor
Ferrocene
LCR

ABSTRACT

Single nucleotide polymorphisms (SNPs) are crucial during the early diagnosis of a given disease as well as in evaluating their response to certain drugs. Thus, this study sought the development of ferrocene (Fc)-labeled electrochemical biosensor for SNP detection. This proposed system involves the ligation of four short probes (e.g., A, B, A′, and B′, where B′ is labeled with an Fc-tag) in the presence of target DNA via ligase chain reaction (LCR), resulting in the formation of Fc-tagged duplex AB-A′B′ in 2^n. Subsequently, immobilization of the Fc-tagged duplex AB-A′B′ on a single-stranded DNA capture probe (SC-DNA)-carboxyl multi-wall carbon nanotube (MWCNT-COOH) modified glassy carbon electrode (GCE) was accomplished through hybridization. Owing to the specificity of hybridization, and the use of Fc as electrochemical probe for detection of duplex AB-A′B′, such strategy realized directly analysis of LCR products without the need for purification. By taking advantage of the thermal stability and high-discrimination ability of HiFi *Taq* DNA ligase for single-base differences, the specificity of hybridization, the *EGFR* T790 M mutant DNA (MT-DNA) biosensor was developed to offer a low limit of detection (0.75 aM), a high discrimination of single-base mismatches [as low as 0.01% (molar fraction)], a wide

* Corresponding author.
** Corresponding author.
E-mail addresses: wangpeng@cpu.edu.cn (P. Wang), guengineering@cpu.edu.cn (Y. Gu).
[1] These authors contributed equally to this work.

https://doi.org/10.1016/j.aca.2020.02.062

linear range of more than 7 orders of magnitude (1 aM–10 pM), and the recovery rates (95.3%–107.8%) from human serum samples. Thus, the biosensor under development was found to be economical, highly-sensitive, and exceptionally selective for detection of SNPs, and as well as extending the versatile applications of LCR to offer great potential for diagnosis and individual clinical regimens.

1. Introduction

Single nucleotide polymorphisms (SNPs) are single-base changes at a specific location in an organism's DNA, which may change the structure and function of encoded proteins, healthy cell regulation, and may cause severe genetic disorders or diseases [1]. Therefore, it is paramount to accurately and rapidly detect SNPs not only for early diagnosis of disease but also for the development of personalized medicine [2–5].

Currently, numerous technologies, such as real-time polymerase chain reaction (RT-PCR) [6,7], next-generation sequencing (NGS) [8], Sanger sequencing [9,10], allele-specific hybridization, magnetic nanoparticle-enzyme sandwich approach [11,12], toehold-mediated strand displacement enzymatic approaches [13], and nanofluidic-embedded biosensors [14], have been applied in identifying SNPs. Nonetheless, the main drawbacks of these technologies are that they are time-consuming and expensive. Thus, there is a growing need for a more economical, sensitive, and rapid approach for detecting SNPs. In recent years, electrochemical detection technology has become an alternative method for detecting SNPs, which has the potential for biosensors development, mainly because it does not require expensive instruments. Numerous electrochemical detection methods based on surfaced modified electrodes (SMEs) have been used for SNP analysis with high-sensitivity, low-cost, and simple instrumentation [15–20]. Also, since the discovery of multi-walled carbon nanotubes (MWCNTs) have demonstrated to be a very efficient sensing material, especially for electroanalytical detection due to its high specific surface area, excellent conductivity, and chemical inertness [21–25]. However, pure MWCNTs tend to fall off the modified electrodes resulting in poor reproducibility and stability. In order to bypass such unwanted characteristics, we utilized Nafion as a more appropriate sensing synergist. Nafion is a perfluorosulfonic acid polymer with ideal properties, for example, electrochemical inactivity, chemical inertness, anti-passivating properties, and hydrophilic. This allowed for the development of a well-dispersed carboxyl multi-wall carbon nanotube/Nafion composite (MWCNT-COOH/Nafion) [26]. We coated this functionalized composite onto a glassy carbon electrode (GCE) surface in order to prepare a stable modified electrode (cMWCNT-NF/GCE). Such preparation provided improvements in the stability and sensitivity of the electrode. We then assembled the amino modified single-stranded DNA capture probes (SC-DNAs) onto the cMWCNT-NF/GCE surface to construct the resulting sensing electrode *via* amide bonds (SC-DNA/cMWCNT-NF/GCE).

Pioneered by the Barany group in 1991, it is worth mentioning that ligase chain reaction (LCR) is a technique developed for DNA-dependent amplification with enzymatic allele discrimination [4,27–30]. Given the high selectivity of the allele-specific enzymatic ligation and targeted recycling during thermal cycles, LCR exhibits superior selectivity and powerful amplification ability, which is optimal for SNP detection. However, LCR-based SNP detection methods remain to be a challenge due to the separation and purification of ligation products. Therefore, by combining LCR with SC-DNA/cMWCNT-NF/GCE, we developed a sensitive biosensor for SNP detection through the hybridization of duplex AB-A′B′ with SC-DNA/cMWCNT-NF/GCE without the need for purification of unreacted Fc-labeled probe B′.

In the treatment of non-small cell lung cancer (NSCLC), the T790 M point mutation in the epidermal growth factor receptor (*EGFR*) gene accounts for nearly 50% of the acquired resistance to *EGFR*-tyrosine kinase inhibitors (TKIs) [31,32]. Thus, identification of *EGFR* T790 M mutation is crucial for choosing further therapeutic strategies during disease progression [33–36].

Herein, we propose a universal LCR-based amplification and electrochemical measuring strategy for SNP detection using *EGFR* T790 M mutant DNA (MT-DNA) as the model analyte. Specifically, the bases of the model analyte at the SNP site are T/A in the MT-DNA and C/G in the wild-type DNA (WT-DNA), respectively. For discrimination of the SNP and detection of MT-DNA, we designed four entirely complementary probes (A, B_{-MT}, A′, and B'_{-MT}) for a typical MT-DNA LCR process. The sequences at the 5′ or 3′-end of the probes were designed to be complementary to the MT-DNA. In particular, probes B_{-MT} and B'_{-MT} were MT-DNA-specific because the bases at the 5′-end of probe B'_{-MT} and the 3′-end of probe B_{-MT} are T and A, which are respectively complementary to the bases of MT-DNA at the SNP site [4,37,38]. Considering the ligation catalyzed by HiFi *Taq* DNA ligase, probes A and B'_{-MT} are modified with a phosphate group at their 5′-end. As illustrated in Scheme 1, there are three key steps involved in our protocol for SNP MT-DNA detection. First, SC-DNA/cMWCNT-NF/GCE was prepared (Scheme 1A). Second, the typical LCR for MT-DNA is illustrated as follows (Scheme 1B): In the presence of MT-DNA, after denaturation at 94 °C, probes A and B_{-MT} pair near their complementary sequences on one template strand at the SNP site by annealing at 60 °C, whereas probes A′ and B'_{-MT} anneal with the second template strand in a similar way. Two adjacent probes are ligated to generate strands AB_{-MT}s and $A'B'_{-MT}$s by the thermostable HiFi *Taq* DNA ligase only when the two probes are perfectly matched to MT-DNA at the junction SNP site. Following subsequent LCR cycles, MT-DNA, the newly formed AB_{-MT}s and $A'B'_{-MT}$s all serve as templates to generate AB-$A'B'_{-MT}$s. In this process, MT-DNA triggers LCR and initiates the exponential amplification of the ligation products, duplex AB-$A'B'_{-MT}$s. In contrast, in the presence of WT-DNA in MT-DNA-special LCR, probes remain unaltered because the mismatched WT-DNA can't trigger LCR (Scheme 1C). By analyzing the LCR products, the MT-DNA and WT-DNA can be differentiated effectively. Lastly, the electrochemical detection strategy is designed (Scheme 1D). To realize the electrochemical measurement, the 21 bases at 5′-end of probe A′ are complementary to SC-DNA and also mismatched with MT-DNA, and ferrocene (Fc, redox indicator for electrochemical detection) was labeled at 3′-end of the probe B'_{-MT}. Subsequently, incubating SC-DNA/cMWCNT-NF/GCE with the LCR products, the duplex AB-$A'B'_{-MT}$s hybridized with SC-DNAs to form the DS-DNA on the electrode surface (DS-DNA/cMWCNT-NF/GCE). Concertedly, Fc is close enough to the electrode surface to produce a voltammetry signal. Only the perfectly matched LCR products generate a detectable current signal of Fc, single-base mismatched products only generate weak electrochemical signals (Scheme 1D). Hence, the DPV signal of Fc can

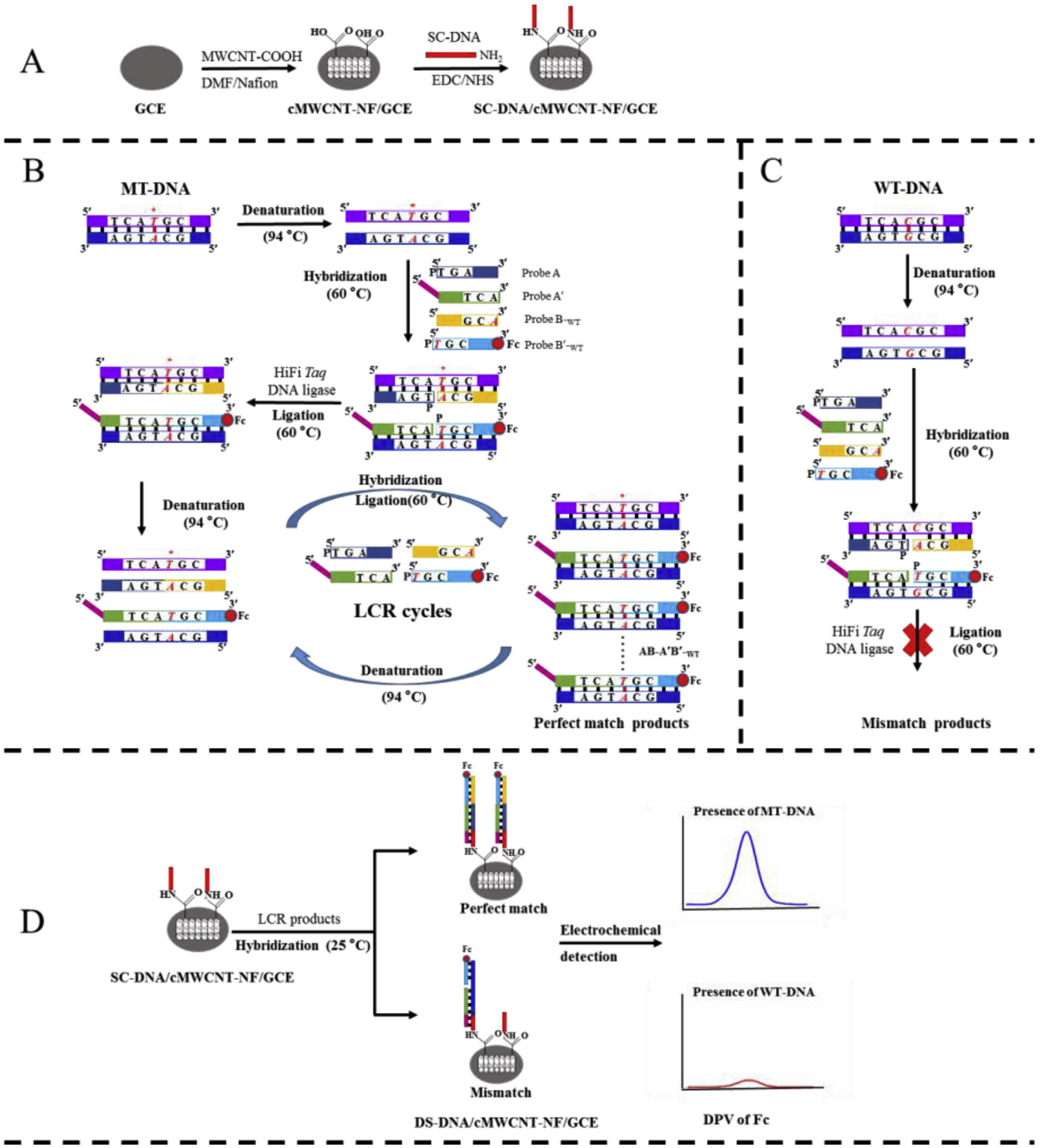

Scheme 1. Schematic illustration of LCR-based MT-DNA electrochemical biosensor. (A) The fabrication of SC-DNA/cMWCNT-NF/GCE. (B) The MT-DNA-specific LCR in presence of MT-DNA. (C) The MT-DNA-specific LCR in presence of WT-DNA. (D) The electrochemical detection protocol of LCR-based MT-DNA electrochemical biosensor. (Fc: ferrocene, electrochemically active indicators).

directly monitor the levels of AB-A′B′$_{-MT}$s and indirectly indicate the levels of the MT-DNA with high specificity.

The innovation of this work is summarized as follows: (1) Based on the high selectivity and high efficiency of HiFi *Taq* DNA ligase, Fc-tagged AB-A′B′ were generated exponentially through LCR in the presence of perfectly matched target DNA. (2) Utilizing the electrochemical probe, Fc, to label MT-DNA-special LCR products, the number of Fc moieties attached to DS-DNA/cMWCNT-NF/GCE electrode surface through hybridization can indirectly monitor the levels of MT-DNA without the need for isolation and

purification. (3) The advantages of hybridization, LCR reaction, as well as the electrochemical testing methods provide high specificity, high selectivity, and high sensitivity for MT-DNA SNP analysis. In summary, our proposed Fc-labeled electrochemical strategy combined with LCR and hybridization provides an economical, purification-free, highly sensitive, and selective detection strategy for SNP genotyping specific to *EGFR* T790 M (MT-DNA).

2. Experimental

2.1. Materials

Polyacrylamide gel electrophoresis (PAGE) kit was purchased from KeyGen Biotech Co., Ltd. (Nanjing, China). MWCNT-COOH with lengths of 10–30 μm was obtained from XFNANO Technology Co., Ltd. (Nanjing, China). HiFi *Taq* DNA ligase and HiFi *Taq* DNA ligase buffer (20 mM Tris-HCl, 150 mM KCl, 10 mM $MgCl_2$, 10 mM DTT, 1 mM NAD, and 0.1% Triton X-100) were purchased from New England Biolabs. Nafion (5% ethanol solution) was purchased from Sigma. *N*-hydroxysuccinimide (NHS), 1-Ethyl-3-(3-dimethylaminopropyl)carbodiimide hydrochloride (EDC), and other chemicals were obtained from Aladdin. (http://www.aladdin-e.com). 6-Mercapto-1-hexanol (MCH) was purchased from Meryer Chemical Technology Co., Ltd. (Shanghai, China). All chemicals were of analytical reagent grade and used without further purification.

All synthetic oligonucleotides were purchased from Shanghai Sangon Biological Engineering Technology and Service Co., Ltd. (Shanghai, China). The *EGFR* T790 M mutation target DNA (MT-DNA) and wild target DNA (WT-DNA), LCR probes (probe A, A′, B_{-MT}, and B'_{-MT} are designed for MT-DNA detection. Probe B_{-WT} and B'_{-WT} are designed for WT-DNA detection), and the amino-modified SC-DNA are listed in Table 1.

All solutions were prepared with ultrapure water.

2.2. Apparatus

Cyclic voltammetry (CV), electrochemical impedance spectroscopy (EIS), and differential pulse voltammetry (DPV) were carried out on a CHI 660C electrochemical workstation (Chenhua Instrument Company Shanghai, China, http://www.chinstruments.com) equipped with a conventional three-electrode system. The conventional three-electrode system consisted of a functionalized glassy carbon electrode (GCE) as the working electrode, a platinum wire as the auxiliary electrode, and a KCl-saturated Ag/AgCl electrode as the reference electrode. CV measurements ranged from −1.0 to 0.5 V at a scan rate of 50 mV s^{-1}. EIS measurements were taken using AC modulation over the frequency range from 0.01 Hz to 100 kHz. DPV scans were incrementally conducted from 0 to 0.6 V at *E* 0.004 V, amplitude 0.05 V, pulse width 0.5 s, and pulse period 0.5 s. All DPVs were baseline-corrected using the application included in software package CHI Version 9.02. All electrochemical experiments were performed at 25 °C.

Scanning electron microscopy (SEM) micrographs were recorded by field-emission scanning electron microscopy (FESEM, Zeiss Ultra Plus). All the LCR amplification were performed with a T100™ Thermal Cycler (Bio-Rad, USA). The gels were visualized by using a Gel Doc™ EZ Imager (Bio-Rad, USA).

2.3. Construction of sensing electrodes

The MWCNT-COOH (4.0 mg ml^{-1}) was dispersed into a DMF solution containing 0.0625% (wt%) Nafion and sonicated for 60 min, which produced the highly dispersed MWCNT-COOH/Nafion suspension. Before surface modification, the GCE was pre-treated to obtain a mirror-like surface, according to a previous study [21]. MWCNT-COOH/Nafion modified the pre-treated GCE for the fabrication of the SNP WT-DNA sensing electrode. Initially, 15 μL of the prepared 4.0 mg ml^{-1} MWCNT-COOH/Nafion suspension was drop-coated onto the pre-treated GCE surface to form a uniform film by subsequently air-drying at 25 °C (cMWCNT-NF/GCE). Next, cMWCNT-NF/GCE was immersed in 200 μL of EDC/NHS (5 mM, 1:1) solution for 12 h to activate carboxyl groups. Subsequently, 15 μL of 20 μM SC-DNA solution was coated onto the activated cMWCNT-NF/GCE for 2 h, followed by the incubation with 10 μM MCH for another 2 h. The amino groups of the SC-DNA at the 3′-end were reacted with the carboxyl groups on the cMWCNT-NF/GCE, and thus an SC-DNA-assembled sensing surface was obtained (SC-DNA/cMWCNT-NF/GCE). The electrode was washed three times with ultrapure water after each step to avoid nonspecific adsorption.

2.4. LCR amplification of MT-DNA

The LCR reaction was performed in a 20 μL solution containing 2 μL of 10 × HiFi *Taq* DNA ligase buffer, 0.5 μL of HiFi *Taq* DNA ligase,

Table 1
Sequences of the oligonucleotides in this study.

DNA name	Sequence (from 5′ to 3′)
MT-DNA	CCTCCACCGTGCAGCTCATCA***T***GCAGCTCATGCCCTTCGGC
WT-DNA	CCTCCACCGTGCAGCTCATCA***C***GCAGCTCATGCCCTTCGGC
Probe A	P-TGATGAGCTGCACGGT
Probe A′	GACTACATAAGCTGGCGTTGGACCGTGCAGCTCATCA
Probe B_{-MT}	AGGGCATGAGCTGC***A***
Probe B'_{-MT}	P-***T***GCAGCTCATGCCCTAAAAA-Fc
SC-DNA	CCAACGCCAGCTTATGTAGTCAAAAA-NH_2
Probe B_{-WT}	AGGGCATGAGCTGC***G***
Probe B'_{-WT}	P-***C***GCAGCTCATGCCCT AAAAA-Fc

The SNP sites are marked with red, italic and bold letter.

20 nM probe A, 20 nM probe B_{-MT}, 20 nM probe A′, 20 nM probe B'_{-MT}, and the appropriate amount of synthetic target DNA (MT-DNA, or WT-DNA). First, the reaction solution was heated at 94 °C for 3 min, then carried out with 30 thermal cycles of denaturation at 94 °C for 30 s, and annealing and ligation at 60 °C for 1 min.

2.5. Hybridization and electrochemical analysis for MT-DNA

Construction of DS-DNA/cMWCNT-NF/GCE by hybridization reaction, 20 μL of WT-DNA LCR products was drop-coated onto the SC-DNA/cMWCNT-NF/GCE surface for 40 min at 25 °C. Subsequently, the construct was gently rinsed three times with ultrapure water. Finally, electrochemical measurements such as CV, EIS, and DPV were immediately performed in 30 min.

3. Results and discussion

3.1. Morphology of electrode

The surface morphology of GCE, cMWCNT-NF/GCE, and SC-DNA/cMWCNT-NF/GCE was examined by SEM to confirm the stepwise modification of the electrode. As shown in Fig. 1, the surface of the GCE was smooth and homogeneous. Whereas the surfaces of cMWCNT-NF/GCE and SC-DNA/cMWCNT-NF/GCE were heterogeneous and rough. MWCNTs-COOH particles were visible in Fig. 1B and C, indicating that MWCNT-COOH had successfully modified the GCE surface [39]. However, the difference between the morphology of cMWCNT-NF/GCE and SC-DNA/cMWCNT-NF/GCE was not observed by SEM.

3.2. Electrochemical performance of the electrode

The specific surface area, electrical conductivity, and the electrostatic interaction of the electrode surface were also characterized by CV and EIS techniques employing $Fe(CN)_6^{3-/4-}$ as a probe [40]. In order to confirm the successful construction of the electrode, CV and EIS measurements at GCE, cMWCNT-NF/GCE, SC-DNA/cMWCNT-NF/GCE, and DS-DNA/cMWCNT-NF/GCE was studied in 5.0 mM $K_3Fe(CN)_6/K_4Fe(CN)_6$ (1:1) solution containing 0.1 M KCl. As shown in Fig. 2A, a pair of well-defined and reversible redox peaks of $Fe(CN)_6^{3-/4-}$ were observed at GCE (black line). Compared with GCE, the peak current at cMWCNT-NF/GCE (red line) increased significantly, which provided evidence for a successful modification of MWCNT-COOH on GCE with high surface area and excellent conductivity. However, a decrease in the peak current was observed for SC-DNA/cMWCNT-NF/GCE (blue line). This can be explained by the negative charges of the SC-DNA phosphate backbone, which hindered the electron transfer and mass transfer of $Fe(CN)_6^{3-/4-}$ anions on the electrode surface. The DS-DNA/cMWCNT-NF/GCE has more negative charges than SC-DNA/cMWCNT-NF/GCE, resulting in a stronger electrostatic repulsion. Hence, the peak signal at DS-DNA/cMWCNT-NF/GCE decreased further (magenta line). The change in peak current of CV proved that the proposed biosensor was successfully assembled as designed. Furthermore, the relevant microscopic surface areas of GCE and cMWCNT-NF/GCE were calculated by CV assays. In a reversible process, the relationship of the anodic peak current i_{pa} versus the scan rate v is given by the Randles—Sevcik equation [41]: $i_{pa} = (2.69 \times 10^5)\, n^{3/2} AD^{1/2} c\, v^{1/2}$, where, A is the surface area of the working electrode, v is the scan rate, c is the concentration of $K_3Fe(CN)_6$, n is number of electrons transferred, $n = 1$ for $K_3Fe(CN)_6$, and D represents the diffusion coefficient, $D = 7.60 \times 10^{-6}$ cm^2 s^{-1}. Therefore, the relative microscopic surface area A of the bare GCE and cMWCNT-NF/GCE calculated by the Randles-Sevcik equation were 0.040 and 0.156 cm^2, respectively. The results proved that the relative microscopic surface area of cMWCNT-NF/GCE had been increased to approximately four times as compared with GCE because of the successful functionalization by MWCNT-COOH. Additionally, EIS is also an important approach for characterizing the electrode surface. Typical EIS spectra generally consist of a semicircle portion at higher frequencies corresponding to electron-transfer limited process and a linear portion at lower frequencies representing the diffusion-limited process. The semicircle diameter in EIS spectra illustrates the charge-transfer resistance (Rct) that controls the electron-transfer kinetics of the redox probe at the electrode interface. Fig. 2B displays the EIS behavior of $Fe(CN)_6^{3-/4-}$ at GCE (red), cMWCNT-NF/GCE (blue), SC-DNA/cMWCNT-NF/GCE (green), and DS-DNA/cMWCNT-NF/GCE (magenta). This figure shows that the Rct of cMWCNT-NF/GCE is much lower than that of GCE, which depicts that MWCNT-COOH improved conductivity at the electrode-electrolyte interface. After immobilization of the SC-DNA, the value of Rct increased, due to the strong electrostatic repulsion interaction between $Fe(CN)_6^{3-/4-}$ and SC-DNA. After the hybridization through incubation of SC-DNA/cMWCNT-NF/GCE with LCR products, stronger electrostatic repulsion increased the Rct of DS-DNA/cMWCNT-NF/GCE continuously. These results are in accordance with CV analysis. Therefore, the EIS assay was employed to quantitatively monitored the construction process of the electrochemical biosensor in our work.

3.3. Feasibility of LCR-based MT-DNA electrochemical biosensor

As mentioned, our proposed electrochemical platform for SNP detection depends on LCR amplification and hybridization. Thus, CV and DPV signals of Fc at DS-DNA/cMWCNT-NF/GCE were studied in a 20 mM Tris-HCl solution to confirm the feasibility of the LCR-based WT-DNA electrochemical biosensor. As shown in Fig. 3A, almost no signal was observed for blank (magenta line, in the

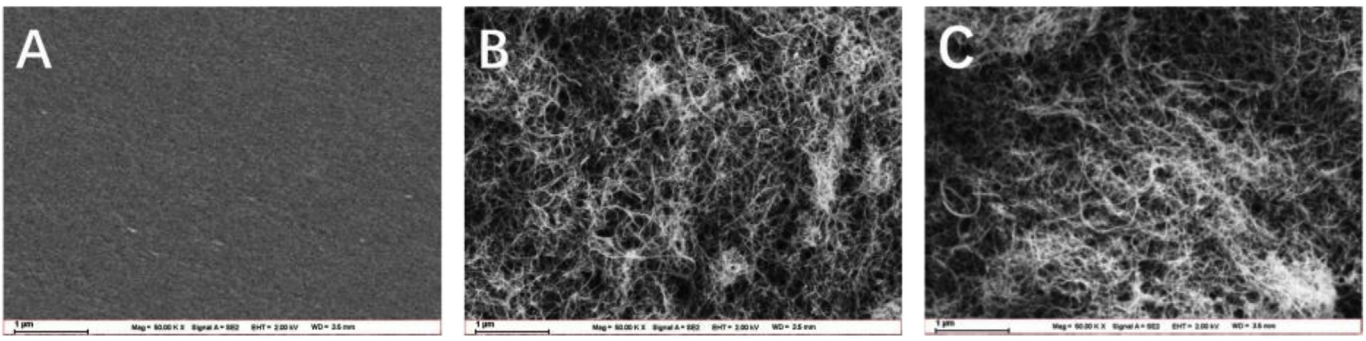

Fig. 1. SEM images of GCE (A), cMWCNT-NF/GCE (B), and SC-DNA/cMWCNT-NF/GCE (C).

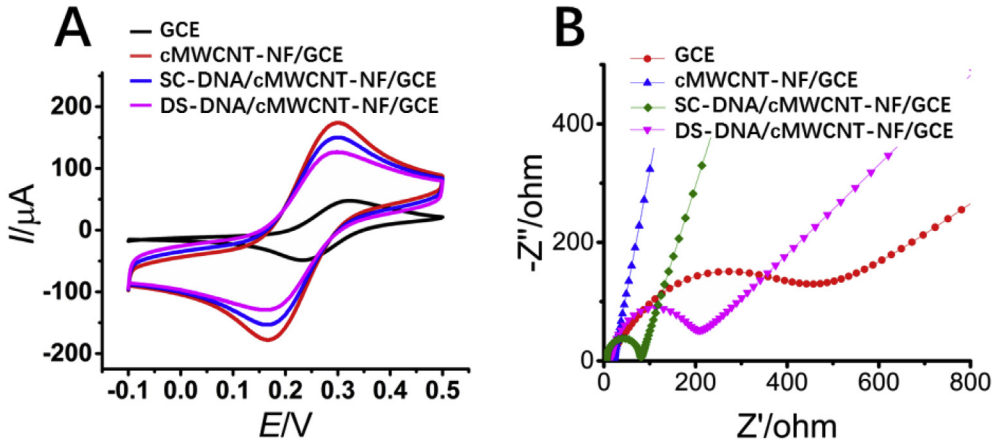

Fig. 2. (A) CV curves and (B) EIS plots of GCE, cMWCNT-NF/GCE, SC-DNA/cMWCNT-NF/GCE and DS-DNA/cMWCNT-NF/GCE.

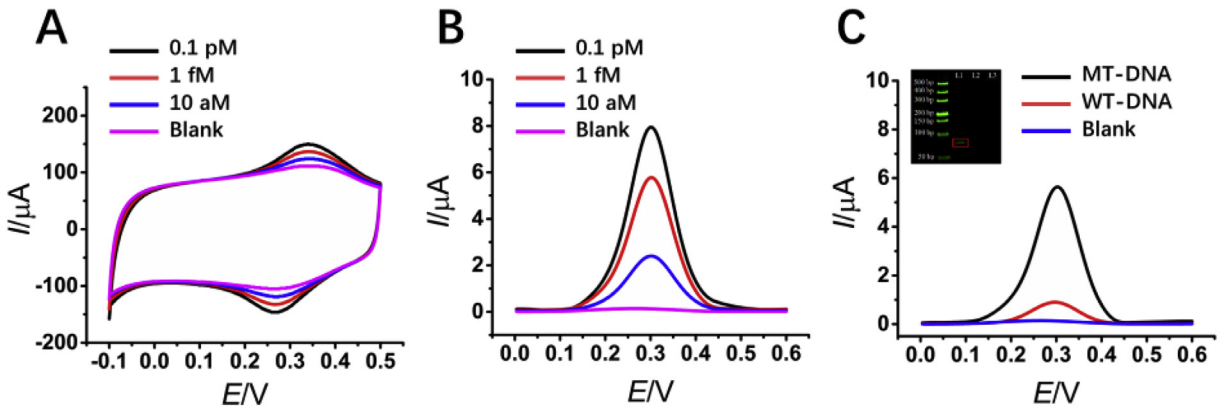

Fig. 3. The feasibility of the LCR-based MT-DNA electrochemical biosensor for MT-DNA detection. (A) CV and (B) DPV responses of MT-DNA electrochemical biosensor to different concentrations of MT-DNA. (C) DPV responses of the MT-DNA electrochemical biosensor for MT-DNA (1 fM), WT-DNA (1 fM), and nagative control (blank). Inset: Results of 8% PAGE of the MT-DNA-special LCR product. M: DNA marker. Lane 1: 1 pM MT-DNA. Lane 2: 1 pM WT-DNA in LCR. Lane 3: negative control.

absence of MT-DNA and WT-DNA in LCR). However, in the presence of MT-DNA in the LCR, a pair of well-defined redox peaks around 0.27 V and 0.34 V were observed for DS-DNA/cMWCNT-NF/GCE, which were attributed to the reduction and oxidation of the Fc molecules. Hence, the Fc molecules labeled at the 3′-end of the probe B'_{-MT} had access to the surface of the electrode through the designed process. In addition, Fig. 3A shows the CV response at DS-DNA/cMWCNT-NF/GCE at 0.1 pM, 1 fM, and 10 aM MT-DNA concentration in MT-DNA-specific LCR, respectively. With the increase of MT-DNA concentration, the signal of Fc increased gradually, indicating that more Fc molecules were bonded to the electrode surface. In order to improve the sensitivity, we chose DPV as the electrochemical measurement because DPV is a more sensitive and effective electrochemical technology than the CV. The DPV response of the Fc molecules modified on DS-DNA/cMWCNT-NF/GCE was measured and shown in Fig. 3B. The magenta line is the DPV response of the blank. The black, red, and blue line represent the DPV response at DS-DNA/cMWCNT-NF/GCE for 0.1 pM, 1 fM, and 10 aM MT-DNA concentration levels of in MT-DNA-specific LCR, respectively. The blank resulted in almost no signal. Compared with CV, the peak current of DPV increased more significantly with increasing MT-DNA concentration. Therefore, DPV was applied for SNP detection in the electrochemical strategy with a higher degree of sensitivity.

Subsequently, the amplification efficiency and differentiation ability of the proposed LCR-based SNP electrochemical strategy was evaluated. Firstly, 1 fM MT-DNA and 1 fM WT-DNA were amplified using the developed MT-DNA-special LCR approach and detected by DPV through our developed electrochemical strategy. The DPV responses of blank (blue), MT-DNA (black), and WT-DNA (red) are shown in Fig. 3C. The peak current intensity in DPV response increases in the presence of MT-DNA and is much stronger than these of the blank and WT-DNA. There was a slight difference between the DPV signals of the blank and WT-DNA. These results indicate an excellent specificity for MT-DNA detection in the MT-DNA-special system. In addition, the MT-DNA amplification products were characterized by 8% PAGE using the SYBR I dye. As shown in Fig. 3C (inset), a band (50–100 bp) was present for the MT-DNA-special LCR system in the presence of MT-DNA (1 pM, L1), whereas there were no bands (50–100 bp) for the MT-DNA-special LCR system in the presence of WT-DNA (1 pM, L2) and blank (absence of MT-T and WT-C, L3). This demonstrated that the base number of the LCR products was consistent with the design and verified the feasibility of the proposed LCR-based MT-DNA electrochemical approach.

In contrast, we also design the probe B_{-WT} and B'_{-WT} to detect WT-DNA by the same method accurately. The bases at the 5′-end of probe B'_{-WT} and the 3′-end of probe B_{-WT} are C and G, which are respectively complementary to the bases of WT-DNA at the SNP site. Therefore, probes B_{-WT} and B'_{-WT} were defined as WT-DNA-specific probes (the sequences of probes are shown in Table 1). As demonstrated in Fig. S1, the differentiation ability of the developed LCR-based SNP WT-DNA electrochemical strategy was verified.

In summary, our proposed LCR-based SNP electrochemical strategy can distinguish and detect target DNA SNP with high sensitivity and specificity.

3.4. Optimization of experimental conditions

In order to achieve high sensitivity and specificity, the concentration of Nafion, the amount of MWCNT-COOH/Nafion suspension, the amount of SC-DNA solution, as well as DPV buffer solution, were carefully optimized. Thus, the well-performing MWCNT-COOH/Nafion dispersion can be easily coated on GCE to construct the cMWCNT-NF/GCE with excellent sensitivity, stability, and reproducibility owing to the synergic effect of MWCNT-COOH and Nafion. The concentration of Nafion and the amount of MWCNT-COOH/Nafion dispersion were optimized according to the difference of $Fe(CN)_6^{3-/4-}$ peak currents between cMWCNT-NF/GCE and SC-DNA/cMWCNT-NF/GCE by CV. From Fig. S2, when the Nafion concentration is higher than 0.0625%, the change of peak currents between cMWCNT-NF/GCE and SC-DNA/cMWCNT-NF/GCE is almost stable. However, when the concentration is 0.0625%, the difference between peak currents rapidly increases to the maximum. The higher the difference in peak current, the better the surface modification by SC-DNA will be. Therefore, 0.0625% Nafion was used as a synergist to improve the stability of biosensor because it not only has an enhanced film-forming ability but also can improve the stability of the sensing electrode by preventing MWCNT-COOH from falling off. Based on the CV response of $Fe(CN)_6^{3-/4-}$ on cMWCNT-NF/GCE (shown in Fig. S3A), the amount of MWCNT-COOH/Nafion dispersion was optimized. The best CV signal was obtained with 15 μL MWCNT-COOH/Nafion dispersion. The CV signal decreases with 20 μL, proving that the electrode surface modification layer is too thick, resulting in its heterogeneity to hinder electron conductivity and mass transfer. Then, we evaluated the amount of 20 μM SC-DNA solution and shown in Fig. S3B. Compared with the cMWCNT-NF/GCE, the peak current slightly decreased with increasing SC-DNA amount and reached a stable electrochemical signal at 15 μL. The above experimental results demonstrated that 15 μL of MWCNT-COOH/Nafion (0.00625% Nafion) did not hinder the reaction site on electrode surface and the carboxyl groups of MWCNTs-COOH were almost completely bonded with SC-DNA-NH_2 (20 μM) at 15 μL. And as shown in Fig. S4, The $Fe(CN)_6^{3-/4-}$ peak current of SC-DNA/cMWCNT-NF/GCE is slightly higher than that of SC-DNA/cMWCNT/GCE. However, it is worth noting that the RSD value of SC-DNA/cMWCNT-NF/GCE is 1.94%, and that of SC-DNA/cMWCNT/GCE is 3.05%, which indicates that SC-DNA/cMWCNT-NF/GCE exhibits highly stable than SC-DNA/cMWCNT/GCE. These results further confirm that Nafion can induce the solubility of MWCNT-COOH and the stability of modified electrodes. The composition of the DPV measuring buffer is also crucial for increasing sensitivity and reproducibility. Therefore, we compared the following two types of running buffers: Tris-HCl (20 mM, pH = 7.2, containing 0.1 M KCl) and PBS (pH = 5.8). As shown in Fig. S5, Tris-HCl produced the perfect DPV signal of Fc. In summary, the optimum experimental parameters were 15 μL of MWCNT-COOH/Nafion (0.00625% Nafion) suspension, 15 μL of 20 μM SC-DNA solution, and Tris-HCl (20 mM, pH = 7.2, containing 0.1 M KCl) buffer solution for DPV.

Furthermore, the retention life of the SC-DNA/cMWCNT-NF/GCE and the optimal measuring time after hybridization at 25 °C were investigated. For the retention life of SC-DNA, the CVs on SC-DNA/cMWCNT-NF/GCE from the 1st to the 50th cycle at a scan rate of 50 mV s^{-1} were obtained and shown in Fig. S6A. There is no difference between these CV signals, confirming that the electrochemical performance of SC-DNA on SC-DNA/cMWCNT-NF/GCE remains unchanged, and the stability of SC-DNA/cMWCNT-NF/GCE is excellent. After hybridization, the DPV of Fc bonded on DS-DNA/cMWCNT-NF/GCE at different times are shown in Fig. S6B. The peak current values were 100%, 98.70%, 97.30%, and 93.90% at 30 min, 60 min, 120 min, and 240 min, respectively, which demonstrated that the electrochemical activity of Fc decreases with time. Therefore, considering the operability of the experimental staff and the safety of the sample, the DPV experiment should be completed in 60 min after hybridization to obtain reliable experimental results.

3.5. Sensitivity and precision of the developed LCR-based MT-DNA electrochemical biosensor

Under the optimized experimental conditions, the sensitivity of the LCR-based MT-DNA electrochemical biosensor is evaluated by using synthetic MT-DNA at different concentrations. As demonstrated in Fig. 4A, increasing the concentration of MT-DNA from 1 aM to 10 pM, the DPV response of Fc increases more rapidly. A calibration plot (Fig. 4B) was obtained by using the peak current (I/μA) versus logarithmic values of concentration ($\lg c_{MT\text{-}DNA}$). The linear relationship was obtained in the range of 1 aM−10 pM, where the equation was $I = 1.44 \lg c_{MT\text{-}DNA} + 27.2$, with $R^2 = 0.9913$. The lower limit of detection (LOD) equals 0.75 aM using $LOD = 3.143\delta_B/S$, where δ_B stands for the standard deviation of the seven responses of blank, and S represents the slope of the calibration curve. As high as 10 pM, the DPV signal almost no longer increases with the increase of MT-DNA concentration because of steric the effect and saturation of hybridization sites. Consequently, our proposed LCR-based MT-DNA electrochemical biosensor achieves excellent sensitivity as low as 0.75 aM and a wide dynamic range of detection more than 7 orders of magnitude.

For any method, it must be repeatable and reproducible. As we know, RSD obtained under the same conditions by an analyst is repeatability, and RSD measured by different analysts is reproducibility. RSD of the results measured is calculated by equation $RSD = (SD \times 100\%)/\bar{x}$, where SD is standard deviation and $\bar{x}$ refers to the arithmetic mean of measuring results. In the presence of 1 fM MT-DNA, the repeatability and reproducibility of our proposed MT-DNA electrochemical biosensor were calculated to be 2.15% and 2.57% (Fig. 5), indicating a high degree of precision.

3.6. Specificity of the developed LCR-based MT-DNA electrochemical biosensor

To determine the specificity of the developed MT-DNA biosensor, the MT-DNA and WT-DNA were mixed at different mole percentages (MT-DNA molar fraction) of 100%, 50%, 10%, 1%, 0.1%, 0.01% and 0% to a total concentration of 500 fM, subsequently serving as target DNA to amplify with MT-DNA-special LCR system. The proposed electrochemical assay analyzed the products. As shown in Fig. 6A, and Fig. 6B, the MT-DNA could be discriminated from the mixture even when the molar percent was as low as 0.01% by the MT-DNA biosensor. Thus, enhanced specificity in discriminating single base mutation from allele mixture was achieved by our LCR-based SNP electrochemical biosensor.

3.7. Universality of LCR-based SNP electrochemical biosensor

The universality of the LCR-based SNP electrochemical strategy was studied through WT-DNA-special system to detect WT-DNA, and results were demonstrated in supporting information. For WT-DNA biosensor, the values of peak current changed linearly with the logarithm of WT-DNA concentration (Fig. S7), which can be described with the equation $I = 1.47 \lg c_{WT\text{-}DNA} + 28.1$ in the range of 1 aM−10 pM ($R^2 = 0.9884$, and LOD = 0.77 aM). Moreover, the repeatability and reproducibility were 2.53% and 2.60%,

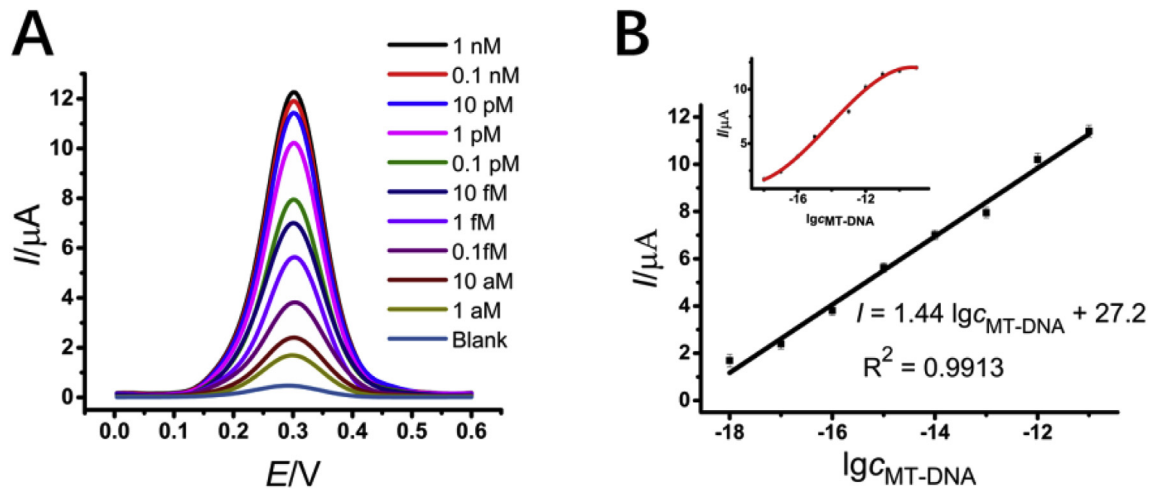

Fig. 4. The sensitivity of the LCR-based MT-DNA electrochemical biosensor for MT-DNA detection. (A) DPV responses of the biosensor to different MT-DNA concentrations. (B) Calibration curve of peak current of DPV verses logarithm of MT-DNA concentration (from 1 aM to 10 pM) (error bars = SD, $n = 3$). Inset: the relationship between the peak current of DPV and logarithm of MT-DNA concentration varying from 1 aM to 1 nM.

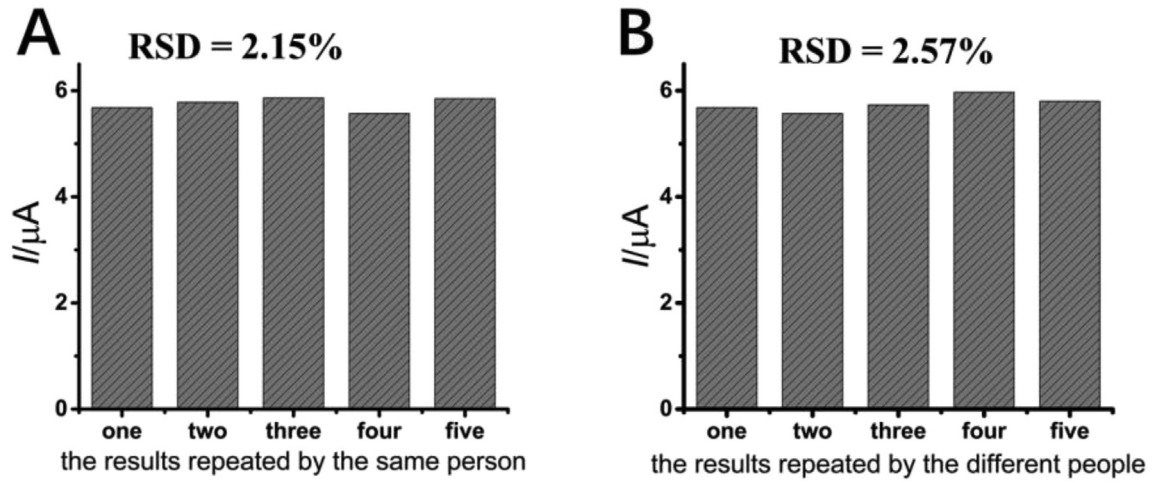

Fig. 5. (A) The repeatability of the LCR-based MT-DNA electrochemical biosensor. (B) The reproducibility of the LCR-based MT-DNA electrochemical biosensor. (1 fM MT-DNA).

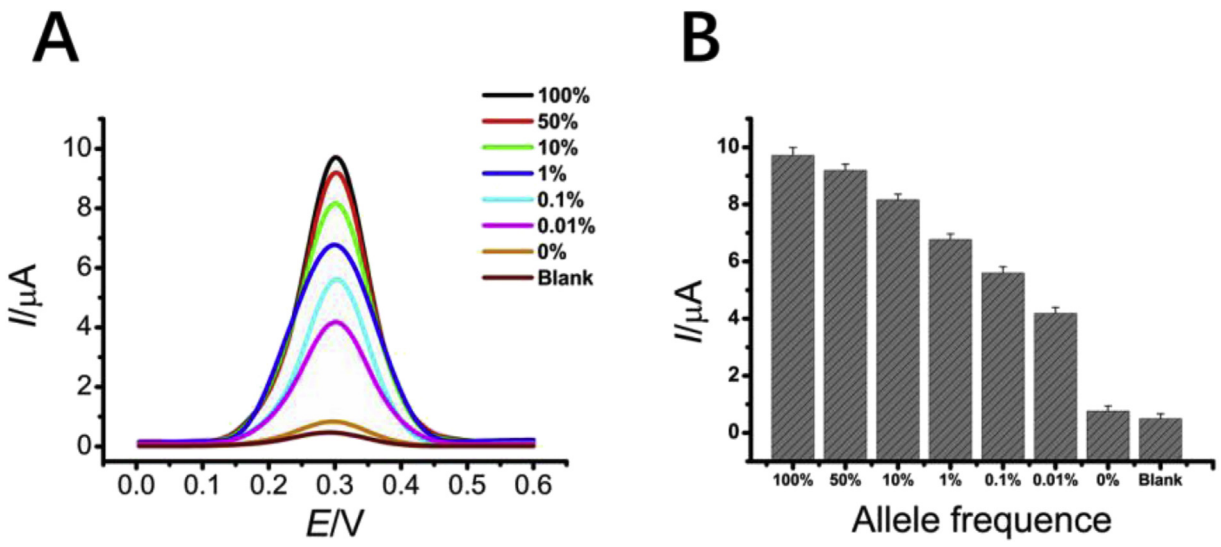

Fig. 6. Specificity of LCR-based MT-DNA electrochemical biosensor. (A) DPV responses of the MT-DNA biosensor produced by mixtures of MT-DNA and WT-DNA with different ratio of MT-DNA to the total DNA (from 100% to 0%). (B) Histogram of DPV peak currents in (A) versus the MT-DNA molar fraction (error bars = SD, $n = 3$). Notes: the total concentration of MT-DNA and WT-DNA was 500 fM.

respectively (Fig. S8). As shown in Fig. S9, the WT-DNA biosensor, detected the target DNA from the WT-DNA and MT-DNA mixture even when the molar percent was as low as 0.01%.

Moreover, in order to study the applicability of the LCR-based SNP electrochemical biosensor in real samples, the recovery rate of synthetic MT-DNA was investigated by adding 100 fM synthetic MT-DNA into human serum through the proposed methodology. As shown in Table S1, the recovery rates of 95.3%–107.8% confirmed that the developed biosensor has high accuracy and reliability. In addition, to investigate the capacity of the developed LCR-based electrochemical biosensor, the content of MT-DNA in the tissue of four patients with non-small cell lung cancer (NSCLC) was determined using this biosensor. The MT-DNA frequency in the tissue of four patients with NSCLC range from 8% to 32%. In particular, the experimental results obtained by our developed biosensor were in good agreement with clinical detection results, indicating the excellent practicability of the developed biosensor for the quantification of MT-DNA in real samples (Fig. S10).

4. Conclusion

Comparing to the double-stranded DNA-assembled electrochemical biosensor using LCR amplification, LCR-electrochemiluminescence emission of quantum dots, real-time fluorescence LCR, rolling circle amplification-responsive G-quadruplex, DNA circuit based amplification-microfluidic chemiluminescence assay and other SNP detection approaches, the LOD and specificity of our developed LCR-based MT-DNA electrochemical biosensor revealed markedly improvements (shown in Table S2).

In summary, combined with LCR and Fc-labeled electrochemical strategy, an economical, purification-free, and universal SNP electrochemical biosensor was developed with high sensitivity and excellent specificity. We constructed the biosensor on the base of the MWCNT-COOH/Nafion composite due to Nafion improving the stability and homogeneity of the sensing surface. Owing to the high fidelity of LCR, enhanced selectivity of hybridization, and satisfactory sensing of the electrochemical platform, the developed MT-DNA biosensor provided a wide dynamic linear range of 7 orders of magnitude (1 aM–10 pM), and with LOD as low as 0.75 aM. Importantly, the developed biosensor discriminated against the target DNA in the allele mixture even when the molar fraction was as low as 0.01%. Also, it detected the target DNA of interest from human serum samples with excellent results. Therefore, the developed biosensor offers potential for the diagnosis of SNP-related diseases and individual clinical regimens.

Declaration of competing interest

The authors declare that they have no known competing financial interests or personal relationships that could have appeared to influence the work reported in this paper.

CRediT authorship contribution statement

Fang Hu: Conceptualization, Investigation, Writing - original draft. **Wancun Zhang:** Methodology, Software, Formal analysis. **Wei Meng:** Validation. **Yuxiang Ma:** Data curation. **Xianwei Zhang:** Visualization. **Ying Xu:** Supervision. **Peng Wang:** Resources, Project administration. **Yueqing Gu:** Writing - review & editing, Funding acquisition.

Acknowledgment

This work was supported by the National Natural Science Foundation Committee of China (NSFC 81729002, 91859204, and 81727804), the 973 Key Project (2015CB755504), and the Fundamental Research Funds for the Central Universities (FY2014LX0038, 2016ZFYX02), Scientific and technological projects of Henan Province (202102310068), Henan Provincial Key Laboratory of Children's Genetics and Metabolic Diseases Foundation.

Appendix A. Supplementary data

Supplementary data to this article can be found online at https://doi.org/10.1016/j.aca.2020.02.062.

References

[1] V.E. Carlton, J.S. Ireland, F. Useche, M. Faham, Functional single nucleotide polymorphism-based association studies, Hum. Genom. 2 (2006) 391–402.
[2] J. Hirschhorn, M. Daly, Genome-wide association studies for common diseases and complex traits, Nat. Rev. Genet. 6 (2005) 95–108.
[3] R.E. Laing, P. Hess, Y. Shen, J. Wang, S.X. Hu, The role and impact of SNPs in pharmacogenomics and personalized medicine, Curr. Drug Metabol. 12 (2011) 460–486.
[4] Q. Xu, K. Chang, W. Lu, W. Chen, Y. Ding, S. Jia, K. Zhang, F. Li, J. Shi, L. Cao, S. Deng, M. Chen, Detection of single-nucleotide polymorphisms with novel leaky surface acoustic wave biosensors, DNA ligation and enzymatic signal amplification, Biosens. Bioelectron. 33 (2012) 274–278.
[5] J. Trinh, E.K. Gustavsson, C. Vilariño-Güell, S. Bortnick, J. Latourelle, M.B. McKenzie, C.S. Tu, E. Nosova, J. Khinda, A. Milnerwood, S. Lesage, A. Brice, M. Tazir, J.O. Aasly, L. Parkkinen, H. Haytural, T. Foroud, R.H. Myers, S.B. Sassi, E. Hentati, F. Nabli, E. Farhat, R. Amouri, F. Hentati, M.J. Farrer, DNM3 and genetic modifiers of age of onset in LRRK2 Gly2019Ser parkinsonism: a genome-wide linkage and association study, Lancet Neurol. 15 (2016) 1248–1256.
[6] D. Husser, V. Adams, C. Piorkowski, G. Hindricks, A. Bollmann, Chromosome 4q25 variants and atrial fibrillation recurrence after catheter ablation, J. Am. Coll. Cardiol. 55 (2010) 747–753.
[7] S. Beinhardt, J.H. Aberle, M. Strasser, E. Dulic-Lakovic, A. Maieron, A. Kreil, K. Rutter, A.F. Staettermayer, C. Datz, T.M. Scherzer, R. Strassl, M. Bischof, R. Stauber, G. Bodlaj, H. Laferl, H. Holzmann, P. Steindl-Munda, P. Ferenci, H. Hofer, Serum level of IP-10 increases predictive value of IL28B polymorphisms for spontaneous clearance of acute HCV infection, Gastroenterology 142 (2012) 78–85, e72.
[8] H. Wakelee, V. Melnikova, C. Karlovich, S. Gadgeel, K. Reckamp, J.W. Goldman, D.R. Camidge, M. Pérol, S.-H. Ou, S. Liu, H. Yu, M. Socinski, T. Mekhail, B. Solomon, R. Natale, G. Otterson, V. Papadimitrakopoulou, J.-C. Soria, C. Langer, J. Neal, D. Despain, S. Yurasov, J. Litten, M. Raponi, M. Erlander, L. Sequist, MA08.01 A highly sensitive next-generation sequencing platform for detection of NSCLC EGFR T790M mutation in urine and plasma, J. Thorac. Oncol. 12 (2017) S384–S385.
[9] D. Pushkarev, N.F. Neff, S.R. Quake, Single-molecule sequencing of an individual human genome, Nat. Biotechnol. 27 (2009) 847–850.
[10] N. Pillay, V. Plagnol, P.S. Tarpey, S.B. Lobo, N. Presneau, K. Szuhai, D. Halai, F. Berisha, S.R. Cannon, S. Mead, D. Kasperaviciute, J. Palmen, P.J. Talmud, L.G. Kindblom, M.F. Amary, R. Tirabosco, A.M. Flanagan, A common single-nucleotide variant in T is strongly associated with chordoma, Nat. Genet. 44 (2012) 1185–1187.
[11] Q. Wang, X. Gan, R. Zang, Y. Chai, Y. Yuan, R. Yuan, An amplified electrochemical proximity immunoassay for the total protein of Nosema bombycis based on the catalytic activity of Fe_3O_4NPs towards methylene blue, Biosens. Bioelectron. 81 (2016) 382–387.
[12] L.D.S. Lapitan, Y. Xu, Y. Guo, D. Zhou, Combining magnetic nanoparticle capture and poly-enzyme nanobead amplification for ultrasensitive detection and discrimination of DNA single nucleotide polymorphisms, Nanoscale 11 (2019) 1195–1204.
[13] L. Li, X. Xiao, J. Ge, M. Han, X. Zhou, L. Wang, X. Su, C. Yu, Discrimination cascade enabled selective detection of single-nucleotide mutation, ACS Sens. 2 (2017) 419–425.
[14] J. Cacheux, M. Brut, A. Bancaud, P. Cordelier, T. Leïchlé, Spatial analysis of nanofluidic-embedded biosensors for wash-free single-nucleotide difference discrimination, ACS Sens. 3 (2018) 606–611.
[15] W.J. Qin, L.Y. Yung, Nanoparticle carrying a single probe for target DNA detection and single nucleotide discrimination, Biosens. Bioelectron. 25 (2009) 313–319.
[16] D.K. Toubanaki, T.K. Christopoulos, P.C. Ioannou, C.S. Flordellis, Identification of single-nucleotide polymorphisms by the oligonucleotide ligation reaction: a DNA biosensor for simultaneous visual detection of both alleles, Anal. Chem. 81 (2009) 218–224.
[17] J. Li, T. Deng, X. Chu, R. Yang, J. Jiang, G. Shen, R. Yu, Rolling circle amplification combined with gold nanoparticle aggregates for highly sensitive identification of single-nucleotide polymorphisms, Anal. Chem. 82 (2010) 2811–2816.
[18] J.Y. Chen, Z.J. Liu, X.W. Wang, C.L. Ye, Y.J. Zheng, H.P. Peng, G.X. Zhong, A.L. Liu,

W. Chen, X.H. Lin, Ultrasensitive electrochemical biosensor developed by probe lengthening for detection of genomic DNA in human serum, Anal. Chem. 91 (2019) 4552–4558.
[19] E.J.H. Wee, S. Rauf, K.M. Koo, M.J.A. Shiddiky, M. Trau, μ-eLCR: a microfabricated device for electrochemical detection of DNA base changes in breast cancer cell lines, Lab Chip 13 (2013) 4385–4391.
[20] G. Liu, R. Lao, L. Xu, Q. Xu, L. Li, M. Zhang, S. Song, C. Fan, Single-nucleotide polymorphism genotyping using a novel multiplexed electrochemical biosensor with nonfoulingsurface, Biosens. Bioelectron. 42 (2013) 516–521.
[21] F. Hu, W. Zhang, J. Zhang, Q. Zhang, T. Sheng, Y. Gu, An electrochemical biosensor for sensitive detection of microRNAs based on target-recycled non-enzymatic amplification, Sens. Actuators, B 271 (2018) 15–23.
[22] A. Star, E. Tu, J. Niemann, J.C. Gabriel, C.S. Joiner, C. Valcke, Label-free detection of DNA hybridization using carbon nanotube network field-effect transistors, Proc. Natl. Acad. Sci. U.S.A. 103 (2006) 921–926.
[23] J.W. Ko, J.M. Woo, A. Jinhong, J.H. Cheon, J.H. Lim, S.H. Kim, H. Chun, E. Kim, Y.J. Park, Multi-order dynamic range DNA sensor using a gold decorated SWCNT random network, ACS Nano 5 (2011) 4365–4372.
[24] J. Tao, P. Zhao, J. Zheng, C. Wu, M. Shi, J. Li, Y. Li, R. Yang, Electrochemical detection of type 2 diabetes mellitus-related SNP via DNA-mediated growth of silver nanoparticles on single walled carbon nanotubes, Chem. Commun. 51 (2015) 15704–15707.
[25] T. García-Mendiola, I. Bravo, J.M. López-Moreno, F. Pariente, R. Wannemacher, K. Weber, J. Popp, E. Lorenzo, Carbon nanodots based biosensors for gene mutation detection, Sens. Actuators, B 256 (2018) 226–233.
[26] J. Wang, M. Musameh, Y. Lin, Solubilization of carbon nanotubes by Nafion toward the preparation of amperometric biosensors, J. Am. Chem. Soc. 125 (2003) 2408–2409.
[27] F. Barany, The ligase chain reaction in a PCR world, PCR Methods Appl. 1 (1991) 5–16.
[28] F. Barany, D.H. Gelfand, Cloning, overexpression and nucleotide sequence of a thermostable DNA ligase-encoding gene, Gene 109 (1991) 1–11.
[29] G.J.S. Lohman, S. Tabor, N.M. Nichols, DNA ligases, Curr. Protoc. Mol. Biol. 94 (2011) 3, 14.1-3.14.7.
[30] A.A. Gibriel, O. Adel, Advances in ligase chain reaction and ligation-based amplifications for genotyping assays: detection and applications, Mutat. Res. Rev. Mutat. Res. 773 (2017) 66–90.
[31] S. Kobayashi, T.J. Boggon, T. Dayaram, P.A. Jänne, O. Kocher, M. Meyerson, B.E. Johnson, M.J. Eck, D.G. Tenen, B. Halmos, *EGFR* mutation and resistance of non-small-cell lung cancer to gefitinib, N. Engl. J. Med. 352 (2005) 786–792.
[32] K.Y. Su, H.Y. Chen, K.C. Li, M.L. Kuo, J.C.H. Yang, W.K. Chan, B.C. Ho, G.C. Chang, J.Y. Shih, S.L. Yu, P.C. Yang, Pretreatment epidermal growth factor receptor (*EGFR*) T790M mutation predicts shorter EGFR tyrosine kinase inhibitor response duration in patients with non-small-cell lung cancer, J. Clin. Oncol. 30 (2012) 433–440.
[33] P. Wang, P. Joshi, A. Alazemi, P. Zhang, Upconversion nanoparticle-based ligase-assisted method for specific and sensitive detection of T790M mutation in epidermal growth factor receptor, Biosens. Bioelectron. 62 (2014) 120–126.
[34] M. Satouchi, H. Tanaka, H. Yoshioka, T. Shimokawaji, K. Mizuno, K. Takeda, I. Yoshino, T. Seto, T. Kurata, N. Tashiro, K. Hagiwara, Detection of epidermal growth factor receptor gene T790M mutation in cytology samples using the cobas® EGFR mutation test, Lung Canc. 111 (2017) 190–194.
[35] K. Yang, J. Li, J. Zhao, P. Ren, Z. Wang, B. Wei, B. Dong, R. Sun, X. Wang, H.J.M. Groen, J. Ma, Y. Guo, Developing ultrasensitive library-aliquot-based droplet digital PCR for detecting T790M in plasma-circulating tumor DNA of non-small-cell-lung-cancer patients, Anal. Chem. 90 (2018) 11203–11209.
[36] R. Zhou, Y. Cai, Z. Li, S. Shen, M. Sha, S.R. Head, Y. Wang, A digital PCR assay development to detect EGFR T790M mutation in NSCLC patients, Front.Lab.Med. 2 (2018) 89–96.
[37] Y. Chen, M. Yang, Y. Xiang, R. Yuan, Y. Chai, Ligase chain reaction amplification for sensitive electrochemiluminescent detection of single nucleotide polymorphisms, Anal. Chim. Acta 796 (2013) 1–6.
[38] W. Zhu, X. Su, X. Gao, Z. Dai, X. Zou, A label-free and PCR-free electrochemical assay for multiplexed microRNA profiles by ligase chain reaction coupling with quantum dots barcodes, Biosens. Bioelectron. 53 (2014) 414–419.
[39] E.K. Savan, Electrochemical determination of N-acetyl cysteine in the presence of acetaminophen at multi-walled carbon nanotubes and nafion modified sensor, Sens. Actuators, B 282 (2019) 500–506.
[40] M.H. Shamsi, H.B. Kraatz, Electrochemical identification of artificial oligonucleotides related to bovine species. Potential for identification of species based on mismatches in the mitochondrial cytochrome C1 oxidase gene, Analyst 136 (2011) 4724–4731.
[41] G.I. Mohammed, N.H. Khraibah, A.S. Bashammakh, M.S. El-Shahawi, Electrochemical sensor for trace determination of timolol maleate drug in real samples and drug residues using Nafion/carboxylated-MWCNTs nanocomposite modified glassy carbon electrode, Microchem. J. 143 (2018) 474–483.